Original Article

Bulletin of Pure and Applied Sciences.
Vol.37 C (Chemistry), No.1, 2018: P.20-26
Print version ISSN 0970 4620
Online version ISSN 2320 320X
DOI 10.5958/2320-320X.2018.00004.3

Investigations of vibrational spectra and bioactivity of ethyl N–[1–(piperidin–1–ylmethyl)benzimidazol–2–yl]carbamate

G.P. Sheeja Mol[1], D. Aruldhas[1,*]

Author Affiliations
[1]Department of Physics & Research Centre, Nesamony Memorial Christian College, Marthandam-629165, TamilNadu, India

Corresponding Author
***D. Aruldhas,** Department of Physics & Research Centre, Nesamony Memorial Christian College, Marthandam-629165, TamilNadu, India

E-mail: aruldhas2k4@gmail.com

Received on 13th January 2018
Accepted on 24th January 2018

Abstract

In this work, FT–IR and FT–Raman spectra of Ethyl N–[1–(piperidin–1–ylmethyl) benzimidazol–2–yl]carbamate have been recorded in the regions 4000–400 cm^{-1} and 3500–50 cm^{-1} respectively. The molecular structure, geometry optimization, intensities and vibrational wave numbers were obtained by DFT levels of theory B3LYP with 6–311G(d,p) standard basis set. The complete vibrational distributions were performed on the basis of the potential energy distribution (PED) of the vibrational energy distribution analysis (VEDA 4) program. The harmonic frequencies were calculated and scaled values were compared with experimental FT–IR and FT–Raman data. The oscillator strength, wavelength and energy were also calculated by TD–DFT method. Molecular electrostatic potential (MESP), total electron density distribution and frontier molecular orbitals (FMOs) are constructed at B3LYP/6311G(d,p) level to understand the electronic properties. The charge density distribution and site of chemical reactivity of the molecules has been obtained by mapping electron density isosurface with electrostatic potential surfaces (ESPs. Ethyl N–[1–(piperidin–1–ylmethyl) benzimidazol–2–yl]carbamate was screened for its antifungal activity.

Keywords: Ethyl N–[1–(piperidin–1–ylmethyl) benzimidazol–2–yl]carbamate, HOMO, LUMO, MESP, Antifungal

1. INTRODUCTION

EthylN–[1–(piperidin–1ylmethyl) benzimidazol–2–yl]carbamate is a systemic agricultural fungicide used to control of certain fungal diseases of stone fruit. Title compound belongs to the family of Benzimidazoles. These are organic compounds containing a benzene ring fused to an imidazole ring. It is a systemic benzimidazole fungicide that is selectively toxic to microorganisms and invertebrates, interfering with cell functions, such as meiosis and intracellular transportation. The selective toxicity of benomyl as a fungicide is possibly due to its heightened effect on fungal rather

than mammalian microtubules [1]. Calmon etal. [2] explained the Kinetics and mechanisms of conversion of methyl 1–(butylcarbamoyl)–2–benzimidazole carbamate (benomyl) to methyl 2–benzimidazolecarbamate (MBC). Decreased permeability as a mechanism of resistance to methyl benzimadazol–2–yl carbamate (MBC) in Sporobolomyces roseus was explained by Nachmias et al. [3]. Van ketel [4] reported the Sensitivity to the pesticide benomyl. Fiscor etal. [5] supported the mutagenicity testing of benomyl, methyl–2–benzimidazole carbamate, streptozotocin and N–methyl–N'–nitro–N–nitrosoguanidine in Salmonella typhimurium in vitro and in rodent host–mediated assays. The main objective of the present study is on the structural analysis of present compound using theoretical and experimental techniques. To the best of our knowledge no detailed spectroscopic studies of these compounds were performed.

2. EXPERIMENTAL

Compound was purchased from Sigma Aldrich (St.Louis, MO, USA) and used without further purification. The room temperature fourier transform infrared spectra of the title compound was measured in the region 400–4000cm^{-1} , at a resolution of +1 cm^{-1}, using Perkin Elmer Spectrometer equipped with mercury vapour lamp and globar as source. The UV-Visible spectra of compound were examined in the range 190–900 nm using CARY100 BIO UV-Visible Spectrometer in acetone solvent. The antifungal activity of compound was analysed by the well diffusion method against the fungi Aspergillus niger and Candida albicans.

2.1. Computational

The combination of spectroscopic methods with DFT calculations are the powerful tools for understanding the fundamental spectral properties and the electronic structure of the compounds. Gaussian 09 software program package was used for theoretical calculation [6]. The quantum chemical calculations were performed by applying density functional theory [7–8] method with the three parameter hybrid functional (B3) [9–10] for the exchange part and the Lee–Yang–Par (LYP) correlation function [11]. The wave number values computed contain known systematic errors and therefore, scaling factor 0.9682 [12] has been used. The potential energy distribution (PED) was calculated with the help of VEDA 4 program package [13]. The Raman activities (S_i) calculated by Gaussian 09 program has been converted to relative Raman intensities (I_i) using the following relationship derived from the basic theory of Raman scattering [14].

$$I_i = \frac{f(\nu_0 - \nu_i)^4 S_i}{\nu_i\left[1 - \exp\left(-\frac{hc\nu_i}{k_b T}\right)\right]}$$

where ν_0 is the exciting wavenumber, ν_i the vibrational wavenumber of the normal mode, h, c and k_b are the universal constants and f is the suitably chosen common normalization factor for all the peak intensities.UV-Visible spectra, electronic tranistions, vertical excitation energies and oscillator strengths were computed with the time-dependent DFT method. Gaussview 5.0.8 visualization program [15] has been utilized to the shape of highest occupied molecular orbital (HOMO) and lowest unoccupied molecular orbital (LUMO).

3. RESULTS AND DISCUSSIONS

3.1. Structural analysis

The optimized molecular structure of compound was performed by using Gaussian 09 program. The results of calculated geometrical parameters (bondlengths, bond angles and dihedral angles) were compared with the experimental values [16–17]. In benzimidazole region, the bondlength C_{12}–N_{11}(1.327Å) shortened while comparing to other C–N bondlengths like C_{12}–N_{13}(1.338 Å) and C_{12}–N_{14} (1.343 Å) due to the influence of N_{14}–H_{15}…O_{24} strong intramolecular hydrogen bonding. The optimized structure of compound as shown in Figure 1.

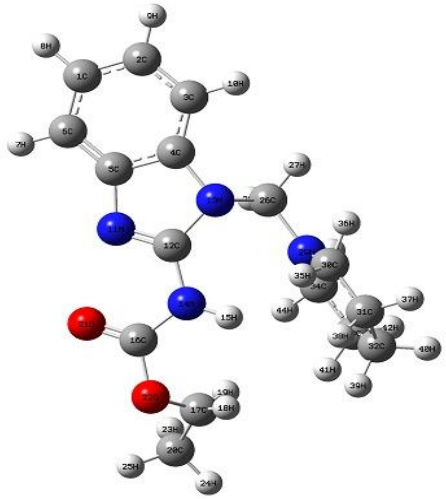

Fig. 1: Optimized molecular structure

The bondlengths N_{11}–C_{12}–N_{13}(109.3°), N_{11}–C_{12}–N_{14}(123.8°) decreases while comparing to N_{13}–C_{12}–N_{14}(127.0°) .In title compound, the dihedral angles N_{11}–C_{12}–N_{14}–H_{15}(–178.8°), N_{11}–C_{12}–N_{14}–C_{16} (1.1°), N_{13}–C_{12}–N_{14}–H_{15}(0.5°) and N_{13}–C_{12}–N_{14}–C_{16}(–179.6°) exhibit the nonplanarity nature of the benzimidazole region.

3.2. Vibrational analysis

The compound consists of 44 atoms, it has 126 normal vibrational modes. The calculations were made for a free molecule in vacuum, while experiments were made for a solid sample. Complete assignments of the fundamentals were propsed based on the calculated PED values. The FT–IR spectrum of compound shown in Figure 2.

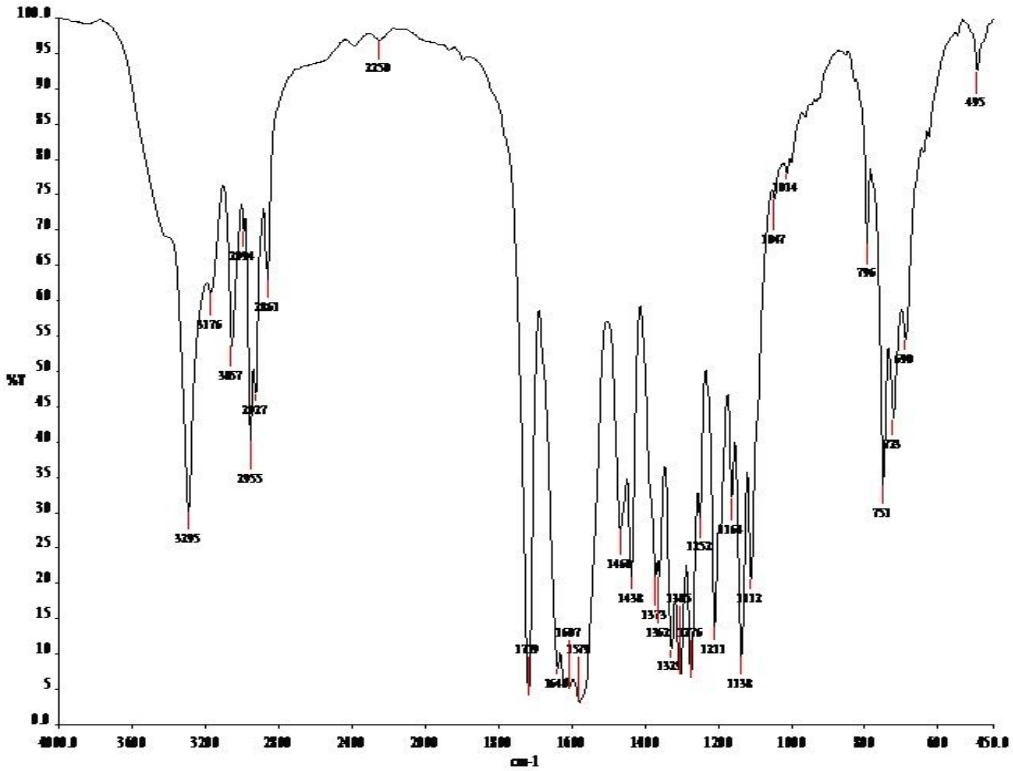

Fig 2: FT–IR Spectrum

3.2.1. N–H vibrations

Normally, in all the heterocyclic compounds, the N–H stretching vibration occurs in the region 3500–3000 cm^{-1} [18]. The band appear at 3295 cm^{-1}in FTIR spectrum is assigned to the N–H stretching mode of the compound.

3.2.2. C=N and C–N vibrations

In general, imidazoles have three or four bands in the regions1660–1450 cm^{-1} due to C=N and C=C stretching vibrations. The intensities of these bands depend on the nature and position of the substituents. Benzimidazoles absorbs at 1560–1520 cm^{-1} due to C=N stretching vibration.. Thus, the band observed at 1487 cm^{-1} is assigned to C=N stretching vibration. The red shift of the C=N stretching frequency of title compound is due to the presents of carbonyl group at C_{12} carbon. The fundamental modes observed at 1398, 1249, 1215 cm^{-1} and 1259cm^{-1} in the IR spectrum, are assigned to C–N stretching modes. The CNC in–plane bending mode is calculated at 957 cm^{-1}. The CNC out of plane bending mode is assigned at 628 cm^{-1} in the IR spectrum. The NCN out of plane bending mode is found at 598 cm^{-1} in IR spectrum. The CCN out of plane bending mode is attributed to 329 cm^{-1} in Raman spectrum.

3.2.3. C–H vibrations

The strong to medium intensity bands occur in the region 3100–3000 cm^{-1} is common for aromatic structure. In the present study, the aromatic C–H stretching vibrations are observed at 3047 cm^{-1} in IR spectrum. The bands due to C–H in–plane bending vibrations occur in the region1290–950 $cm^{-1.}$ The bands observed at 1154, 1124, 1008 cm^{-1} in IR spectrum are assigned to C–H in–plane bending vibrations of the molecule. The C–H out of plane bending modes is usually medium intensity and is observed in the region 950–600 $cm^{-1.}$ The out of plane C–H bending vibrations are observed at 931 and 851 cm^{-1} in IR spectrum.

3.2.4. C–C vibrations

The ring C–C stretching vibrations occur in the region 1650–1430 cm^{-1} [19]. In the present study, the C–C stretching vibrations of compound are observed at 1629 and 1596 cm^{-1} in the infrared spectrum. The C–C stretching vibrations are assigned to the modes 1353 and 1314 cm^{-1}in the IR .The ring CCC in–plane bending vibrations are generally weak often being masked by other stronger absorptions due to the substituent groups. The in–plane bending vibrations of compound are theoretically determined at 891, 808, 582 $cm^{-1}$and the calculated out of plane vibrations are 431, 392, 249, 139 and 101 $cm^{-1.}$These assignments are in good agreement with literature.

3.3 UV–visible spectral analysis

Electronic transitions have been investigated by UV–Visible spectroscopy. Absorption maximum (λ_{max}) was calculated by TD–DFT method. The experimental UV–Visible absorption spectrum of the sample is shown in figure 3. The UV–Visible spectrum was measured in acetone and it is found that the absorption bands are observed at 210nm. A very strong band at 210nm is a characteristic peak of aromatic system due to $\pi \rightarrow \pi^*$ transition.

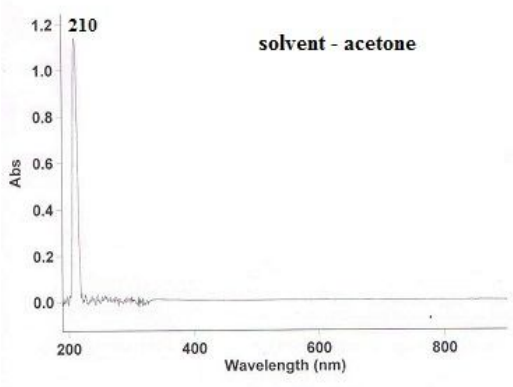

Fig. 3: UV–Visible spectrum

3.4 HOMO–LUMO ANALYSIS

Molecular orbitals, both the highest occupied molecular orbital (HOMO) and the lowest unoccupied molecular orbital (LUMO) and their properties such as energy are very useful for physicists and chemists are the main orbital taking part in chemical reaction while the energy of the HOMO is directly related to the ionization potential, LUMO energy is directly related to the electron affinity [20–21]. This is also used by the frontier electron density for predicting the most reactive position in π–electron system and also explains several types of reaction in conjugated system [22]. The conjugated molecules are characterized by a small highest occupied molecular orbital–lowest unoccupied molecular orbital separation, which is the result of a significant degree of intramolecular charge transfer from the end–capping electron–donor groups to the efficient electron–acceptor group through π–conjugated path[23]. Surfaces for the frontier orbitals were drawn to understand the bonding scheme of compound1 and it's related compounds. The energy difference between HOMO and LUMO orbital which is called as energygap is a critical parameter in determining molecular electrical transport properties because it is a measure of electron conductivity.

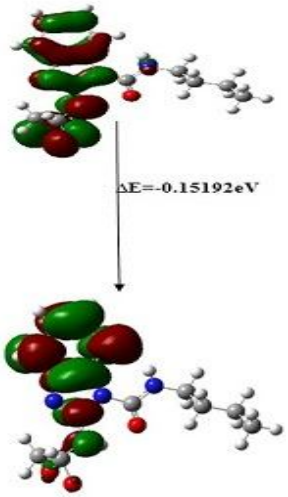

Fig. 4: HOMO–LUMO ENERGY GAP

3.5. MESP

The electrostatic potential is also well suited for analyzing processes based on the "recognition" of one molecule by another, as in drug–receptor, an enzyme–substrate interactions, because it is through their potentials that the two species first "see" each other [24–25]. To predict reactive sites of electrophilic and nucleophilic attacks for the investigated molecule, MESP at the B3LYP/6–311G (d,p) optimized geometry was calculated. The negative (red and yellow) regions of MESP were related to electrophilic reactivity and the positive (blue) regions to nucleophilic reactivity (Fig.5). The predominance of green region in the MESP surfaces corresponds to a potential halfway between the two extremes red and blue colour. As can be seen from the MESP map of the title compound, negative regions are mainly localized over the carbonyl groups The maximum positive regions are localized over the benzimidazole ring. As can be seen from the MESP map, regions having the negative potentials are over the electronegative atoms.

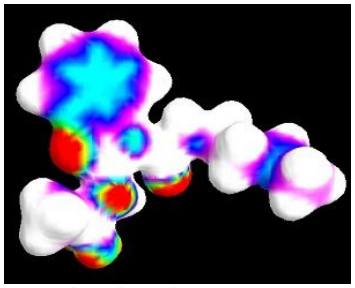

Fig. 5: Molecular Electrostatic potential

3.6. Antifungal activity

The antifungal activity of title compound lwere evaluated by the well–diffusion method against the fungi viz, Aspergillus niger and candida albicans cultured on potato dextrose agar as medium. The stock resolution was prepared by dissolving the compounds in DMSO and the solutions were serially diluted to find MIC (Minimal Inhibitory Concentration) values wells of approximately 10 mm was bored using a well cutter and samples of different concentration was added. The zone of inhibition was measured after overnight incubation and compared with that of standard antibiotics. The well was filled with the test solution using a micropipette and the plate was incubated 72H for fungi at 35 °C. During this period the test solution diffused and the growth of the inoculated microorganisms was affected. The inhibition zone was developed, at which the concentration was noted [26].The antifungal and solvent test for fungal strains were increased and mentioned in Table 1. It is noticed that itself has no activity on the figure.

Table 1: In vitro Antifungal activity

Sl. No.	Fungal pathogen	Zone of inhibition(mm)			
		250(µg)	500(µg)	1000(µg)	Clotrimazole(µg)
1	Aspergillus niger	15	25	25	30
2	Candida albicans	nil	nil	15	27

The experimental values show considerable activity observed in candida albicans against aspergillus niger, Clotrimazole as the standard drug used for this study. The inhibitory activity of the synthesized compound on the organism shows high activity in high concentration of the title compound increases; the inhibition of fungal strains also increases. Figure 6(a) and 6(b) indicates the antifungal activity of title compound at different concentrations for two antifungal pathogens (aspergillus niger and candida albicans). The presence of benzimidazole region in title compound is responsible for the antifungal action.

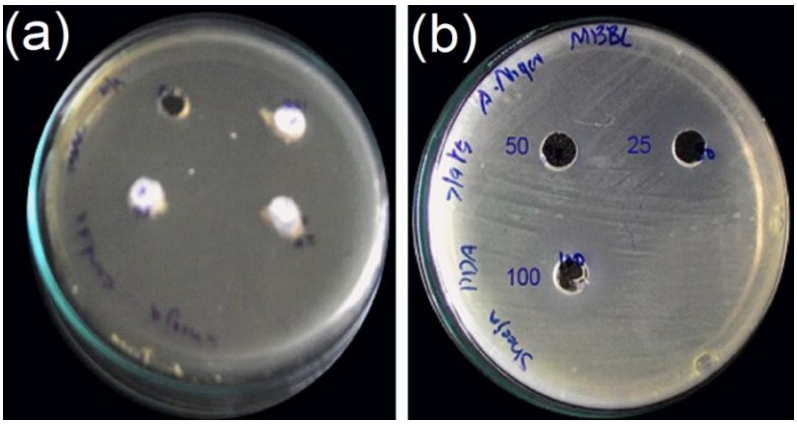

Fig. 6: Antifungal activity with (a) aspergillus niger and (b) candida albicans

5. CONCLUSIONS

In the present work, the optimized geometric parameters (bondlengths, bond angles and dihedral angles) were theoretically determined and compared with the experimental results. The increase in wavenumber from the expected value leads to the redshift and exhibits the possibility of intramolecular hydrogen bonding. The lowering of HOMO-LUMO bandgap supports fungicidal activity of title compound. The experimental UV-Visible spectrum shows an absorption maxima at 210 nm($n \rightarrow \pi^*$) in the acetone solvent. The maximum positive regions are localized over the benzimidazole region. Thus from above investigations, it can be concluded that title compound is a good antifungal agent to treat diseases and further work can be responsible for biological activity.

REFERENCES

[1] EPA: Federal Register: Benomyl; Cancellation Order (http://www.epa.gov/EPA–PEST/2001/August/Day–08/p19572.htm).
[2] Calmon J.P., Sayag D.R., J Agric. Food Chem., 24(2), **1976,** 311–314.
[3] Nachmias A., Barash I, J. Gen. Microbiol., 94(1), **1976,** 167–172.
[4] Van Ketel W.G., Contact Dermatitis, 2(5), **1976,** 290–291.
[5] Ficsor G., Bordas S., Stewart S.J., Mutat Res., 51(2), **1978,** 151–164.
[6] Frisch M.J., Trucks G.W., Schlegel H.B., Gaussian 09W Program, Gaussian Inc., Wallingford, CT, , **2009**.
[7] Camargo A.J., Napolitano H.B., Schpector J.Z., J. Mol. Strut.: Theochem., 816(1), **2007,** 145–151.
[8] Arul Dhas D., Hubert Joe I., Roy S. D. D., Balachandran S., Spectro.chim Acta Part A, 135, **2015,** 583–596.
[9] Becke A. D., J. Chem. Phys., 98, **1993,** 5648–5652.
[10] Becke A. D., Phys. Rev. A, 38, **1988,** 3098–3100.
[11] Lee C., Yang W., Parr R.G., Phy. Rev. B, 37, **1988,** 785–789.
[12] Merrick J.P., Moran D., Radom L., J. Phy. Chem A, 111, **2007,** 11683–11700.
[13] Jamroz M.H., Vibrational energy distribution analysis VEDA 4, Warsaw, Poland, , **2004**.
[14] Keresztury G., Holly S., Besengei J.V., Wang A.Y., Spectrochimica Acta Part A, 49, **1993,** 2007–2026.
[15] Denningten R., Keith T., Millam J., Gaussview version 5.0.8, Gaussian, Inc, 235 wallingford CT, **2009**.
[16] Sepassi K., Nichol G.S. and Yalkowsky S.H., Acta cryst. E62, **2006,** 05172–05173.
[17] Mao–sen yuan and Qi Fang, Acta cryst., E67, **2011,** 52.
[18] Socrates G., Infrared and Raman characteristic group frequencies, tables and charts, 3rd ed., Wiley, Chichester, **2001**.
[19] Sathyanarayana D.N., Vibrational Spectroscopy—Theory and Applications, 2nd ed., New Age International (P) Limited Publishers, New Delhi, **2004,**
[20] Fukui, Science, 218, **1982,** 747–754.
[21] Gunasekaran G., Balaji R.A., Kumaresan S. , Anand G. , Srinivasan S., Can. J. Anl. Sci. Spectrosc., 53, **2008,** 149–162.
[22] Fukui K., Yonezawa T., Shingu H., J. Chem. Phys., 20, **1952,** 722–725.
[23] Choi C.H., Kertesz M., J. Phys. Chem., 101, **1997,** 3823–3831.
[24] Politzer P., Murray J.S., heoretical Biochemistry and Molecular Biophysics: A Comprehensive Survey, Vol.2, Adenine Press, Schenectady, Newyork D.L.Beveridge, R. Lavery (Eds.), **1991**.
[25] Scrocco E., Thomasi J., Top. Curr. Chem., 42, **1973,** 95–170.
[26] Raman N., Dhaveethu Raj J., Sakthivel A., J. Chem. Sci., 119, **2007,** 303–310.